THE JOURNAL OF BIOLOGICAL CHEMISTRY VOL. 290, NO. 9, pp. 5241–5255, February 27, 2015

Proteolytic Regulation of Epithelial Sodium Channels by Urokinase Plasminogen Activator

*CUTTING EDGE AND CLEAVAGE SITES**

Received for publication, November 4, 2014, and in revised form, December 17, 2014 Published, JBC Papers in Press, January 2, 2015, DOI 10.1074/jbc.M114.623496

Hong-Long Ji[‡§1], Runzhen Zhao[‡], Andrey A. Komissarov[‡], Yongchang Chang[¶], Yongfeng Liu[‖], and Michael A. Matthay[**]

*From the [‡]Department of Cellular and Molecular Biology and the [§]Texas Lung Injury Institute, University of Texas Health Science Center, Tyler, Texas 75708, the [¶]Barrow Neurological Institute, St. Joseph's Hospital and Medical Center, Phoenix, Arizona 85013, the [‖]College of Public Health, Xinxiang Medical University, Xinxiang, Henan 453100, China, and the **Departments of Medicine and Anesthesia, Cardiovascular Research Institute, University of California, San Francisco, California 94143*

Background: Depressed fibrinolysis and edema concurrently exist in edematous injury.
Results: Divergent regulation of ENaC by urokinase and tPA was observed. Both the catalytic domain of urokinase and cleavage sites in ENaC were identified.
Conclusion: Urokinase activates ENaC through catalytic activity-dependent proteolytic modification of γ subunit.
Significance: Activation of ENaC by urokinase but not tPA provides a novel mechanism for the alleviation of lung edema and pleural effusion.

Plasminogen activator inhibitor 1 (PAI-1) level is extremely elevated in the edematous fluid of acutely injured lungs and pleurae. Elevated PAI-1 specifically inactivates pulmonary urokinase-type (uPA) and tissue-type plasminogen activators (tPA). We hypothesized that plasminogen activation and fibrinolysis may alter epithelial sodium channel (ENaC) activity, a key player in clearing edematous fluid. Two-chain urokinase (tcuPA) has been found to strongly stimulate heterologous human αβγ ENaC activity in a dose- and time-dependent manner. This activity of tcuPA was completely ablated by PAI-1. Furthermore, a mutation (S195A) of the active site of the enzyme also prevented ENaC activation. By comparison, three truncation mutants of the amino-terminal fragment of tcuPA still activated ENaC. uPA enzymatic activity was positively correlated with ENaC current amplitude prior to reaching the maximal level. In sharp contrast to uPA, neither single-chain tPA nor derivatives, including two-chain tPA and tenecteplase, affected ENaC activity. Furthermore, γ but not α subunit of ENaC was proteolytically cleaved at (^{177}GR ↓ KR^{180}) by tcuPA. In summary, the underlying mechanisms of urokinase-mediated activation of ENaC include release of self-inhibition, proteolysis of γ ENaC, incremental increase in opening rate, and activation of closed (electrically "silent") channels. This study for the first time demonstrates multifaceted mechanisms for uPA-mediated up-regulation of ENaC, which form the cellular and molecular rationale for the beneficial effects of urokinase in mitigating mortal pulmonary edema and pleural effusions.

Urokinase-type plasminogen activator (uPA)[2] initiates fibrinolysis by converting plasminogen to plasmin. In the respiratory system, uPA is expressed in the airway epithelium, alveolar epithelial cells, macrophages, and pulmonary capillary endothelial layer (1–6). uPA released from these cells is a single-chain molecule (scuPA), which can be further proteolytically cleaved to form active two-chain enzyme (tcuPA). uPA is readily detectable in bronchoalveolar lavage and pleural fluid in mammals and is a primary contributor of fibrinolytic activity in lungs (3, 7, 8). Tissue-type plasminogen activator (tPA), however, is not expressed in lung epithelial tissues and cannot be detected in luminal fluid lining the airways and air sacs. Both uPA and tPA are endogenous plasminogen activators. To maintain fibrinolytic homeostasis, inhibitors of plasminogen activators 1 and 2 (PAI-1 and PAI-2) and plasmin (α_2-antiplasmin and α_2-macroglobulin) coordinately fine tune the plasminogen activation system.

The balance between plasminogen activators and their corresponding inhibitors is disrupted in edematous lungs and pleural injuries, including acute lung injury, acute respiratory distress syndrome, high altitude pulmonary edema, and pleural effusions (1, 9, 10). Accumulating evidence from clinical studies and animal models has confirmed a depression in plasminogen activation in bronchoalveolar lavage or pleural fluid (11–13). This is primarily attributable to a tremendous elevation in PAI-1 level (a prognostic biomarker) and a significant reduction in uPA and plasmin (14–18). Concurrently, the balance

* This work was supported, in whole or in part, by National Institutes of Health Grants HL87017 and HL095435. This work was also supported by American Heart Association Grant 14GRNT20130034 and an institutional fund from the University of Texas Health Science Center at Tyler Research Council.
[1] To whom correspondence should be addressed: 11937 U.S. Hwy. 271, 604 BMR, Tyler, TX 75708-3154. Fax: 903-877-5438; E-mail: james.ji@uthct.edu.

[2] The abbreviations used are: uPA, urokinase-type plasminogen activator; tPA, tissue-type plasminogen activator; scuPA and sctPA, single-chain uPA and tPA, respectively; tcuPA and tctPA, two-chain uPA and tPA, respectively; uPAR, uPA receptor; ENaC, epithelial sodium channel; PAI, plasminogen activator inhibitor; CPD, connecting peptide; GFD, growth factor domain; TNK, tenecteplase; MTSET, 2-(trimethylammonium)ethyl methanethiosulfonate bromide; ATF, amino-terminal fragment; HMW, high molecular weight; LMW, low molecular weight; cRNA, complementary RNA; AU, arbitrary units; Tricine, *N*-[2-hydroxy-1,1-bis(hydroxymethyl)-ethyl]glycine.

between fluid turnover and resolution in the airways, alveolar spaces, and pleural cavity is lost. Accumulation of edematous fluid mainly results from fluid reabsorption that cannot be compensated for by fluid leakage (19–21). This pathogenic scenario can be illustrated with alveolar fluid clearance. Alveolar fluid removal is driven by the osmotic sodium gradient as well as electrical potential difference across the alveolar epithelium. Vectorial transalveolar salt transport generates both chemical and electrical differences between luminal and interstitial compartments. Epithelial sodium channels (ENaC) at the apical membrane and ATP-consuming Na^+/K^+-ATPase at the basolateral membrane coordinately control sodium inward movement and depolarize the epithelial layer (22, 23).

Reduced ENaC expression and activity have been described in both edematous pulmonary diseases and animal models (19, 24). Defective lung fluid clearance has been confirmed in mice with deficient *scnn1* genes (25). uPA and tPA decreased the severity of lung injury and pleural effusion (26–32). Whether delivered plasminogen activators evoke ENaC-mediated edema resolution, however, is unknown to date.

The concurrent edema formation and suppressed fibrinolysis in injured lung and pleural cavity suggest a potential contribution of fibrinolysis to ENaC function. Indeed, ENaC activation by plasmin has been recently demonstrated (33, 34). Both uPA (abbokinase) and tPA (alteplase) are extensively used for fibrinolytic therapy for asthma, pleural effusion, and other respiratory diseases. However, to the best of our knowledge, the effects and underlying mechanisms of tPA and uPA on ENaC function remain obscure. This study therefore aims to understand the molecular pharmacological mechanisms by which these serine proteases resolve edema fluid. Herein we determined whether tPA and uPA affect ENaC activity. Electrical measurements of amiloride-inhibitable sodium ion flow were used to determine channel opening status upon exposure to plasminogen activators. Human tcuPA, but not tPA nor tenecteplase (TNK), activates human $\alpha\beta\gamma$ ENaC expressed in *Xenopus* oocytes. The catalytic domain of tcuPA is responsible for its stimulatory effects. Furthermore, tcuPA releases self-inhibition, increases activation rate, and activates electrically "silent" channels. γ ENaC is proteolytically cleaved by tcuPA through hydrolysis of a unique domain. Activation of ENaC specifically by uPA may contribute to fluid clearance under physiological conditions and in injured tissues. These are novel mechanisms for uPA whereby it could be an effective clinical intervention in edematous respiratory injury.

EXPERIMENTAL PROCEDURES

Proteins and Reagents—Wild type (WT) uPA, truncated mutants (ΔGFD, Δkringle, and ΔCPD) and a site-directed mutant (S195A) of uPA, and PAI-1-resistant TNK-tPA were obtained from Attenuon LLC (San Diego, CA) or were produced and purified as described (35, 36). By convention, these proteases are numbered based on the chymotrypsin sequence numbers. Human recombinant WT sctPA was obtained from Genentech (South San Francisco, CA). High (HMW) and low molecular weight (LMW) tcuPA compounds were obtained from Abbott. HMW tcuPA activity standard (100,000 IU/mg) was purchased from American Diagnostica (Stamford, CT). The concentrations of proteins were calculated either from absorbance at 280 nm (uPA, tPA, and PAI-1), using M_r of 54,000, 63,500, and 43,000 and $\epsilon^{1\%}_{280}$ of 1.36, 1.90, and 0.93, or from measurements with a BCA protein assay kit (Pierce).

Measurements of uPA and tPA Amidolytic Activity—Amidolytic uPA and tPA activity was determined using fluorogenic substrates (Pefafluor uPA and Pefafluor tPA, respectively; Centerchem, Basel, Switzerland). Aliquots (10–25 μl) of samples were mixed with 0.05 M HEPES buffer (pH 7.4, 20 mM NaCl, 50 μl) in 96-well white flat bottom Costar plates (Corning Inc.). 50 μl of 100 μM Pefafluor uPA or 200 μM Pefafluor tPA in the same buffer were added to each well and mixed. Time traces of changes in the fluorescence emission at 440 nm (excitation 344 nm) in each well were registered using a Varian Cary Eclipse fluorescence spectrophotometer equipped with a 96-well plate reader accessory (Varian Inc.). The results were fitted to a linear equation using Varian software to determine the rates of substrate hydrolysis, which were recalculated to arbitrary units (AU) of enzymatic activity. Amidolytic enzyme activities were analyzed using Varian Eclipse Kinetic software. S.E. values were less than 10%.

Conversion of Single-chain Proenzymes into Two-chain Mature Form—Single-chain uPA was converted to the two-chain form by incubation with immobilized plasmin (Molecular Innovations), as described previously (37). scuPA could also be cleaved by plasmin at Lys^{158}-Ile^{159} to produce potent tcuPA, accompanied by a conformational change in proteins. As shown in Fig. 2*B* (*top*, *inset*), a single disulfide bond connects the amino-terminal A-chain to the catalytically active, carboxyl-terminal B-chain. This two-chain derivative is also called HMW uPA. HMW uPA can be further processed into LMW uPA by cleavage of chain A into a short amino-terminal fragment. LMW-uPA is proteolytically active but does not bind to the uPA receptor. scuPA and its mutant variants were converted to the two-chain mature form by treatment with immobilized plasmin. Enzymes (1–5 mg) were incubated with plasmin-agarose (0.1–0.4 ml) at 37 °C in 0.5–2.0 ml of 0.1 M HEPES (pH 7.4). Aliquots were withdrawn to monitor amidolytic activity using fluorogenic substrate Pefafluor uPA. As soon as enzymatic activity in the preparation peaked, resin was removed, and enzyme was precipitated with ammonium sulfate, dissolved in 0.1 M HEPES, pH 7.4, passed through a P-10 gel filtration column, aliquoted, and stored at −80 °C. The conversion (more than 95%) of single-chain enzymes to the two-chain form and the absence of degradation were confirmed by SDS-PAGE under reducing conditions (4–12% gradient gel, NuPage; Invitrogen) using the XCell SureLock Mini-Cell (Invitrogen).

Construction of ENaC Mutants—Deletion and site-directed mutants were generated in human γ ENaC cDNA cloned into pGEM HE vector using the QuikChange II site-directed mutagenesis kit (Stratagene) (38, 39). cRNAs of human α, β, and γ ENaC were prepared as described previously (40).

Oocyte Expression and Voltage Clamp Studies—Oocytes were surgically removed from appropriately anesthetized adult female *Xenopus laevis* (*Xenopus* Express). Briefly, the ovarian tissue was removed from frogs under anesthesia by ethyl 3-aminobenzoate methanesulfonate salt (Sigma) through a small incision in the lower abdomen. Ovarian lobes were removed

and digested in OR-2 calcium-free medium (82.5 mM NaCl, 2.5 mM KCl, 1.0 mM $MgCl_2$, 1.0 mM Na_2HPO_4, and 10.0 mM HEPES, pH 7.5) with the addition of 2 mg/ml collagenase (Roche Applied Science). Defolliculated oocytes were injected with ENaC cRNAs into the cytosol (25 ng/oocyte in 50 nl of RNase-free water) and incubated in regular OR-2 medium at 18 °C. The two-electrode voltage clamp technique was used to record whole-cell currents 48 h postinjection. Oocytes were impaled with two electrodes filled with 3 M KCl, having resistance of 0.5–2 megaohms. A TEV-200 voltage clamp amplifier (Dagan) was used to clamp oocytes with concomitant recording of currents. Two reference electrodes were connected to the bath. The continuously perfused bathing solution was ND-96 medium (96.0 mM NaCl, 1.0 mM $MgCl_2$, 1.8 mM $CaCl_2$, 2.5 mM KCl, and 5.0 mM HEPES, pH 7.5). Whole-cell currents were recorded as reported previously (41). Experiments were controlled by pCLAMP version 10.1 software (Molecular Devices), and currents at −40, −100, and +80 mV were continuously monitored with data recorded at intervals of 10 s. Data were sampled at a rate of 200 Hz and filtered at 500 Hz.

To study the effects of fibrinolytic proteases on ENaC activity, both WT and mutant uPA and tPA were incubated with oocytes in serum-free OR-2 medium over a time course followed by measurements of whole-cell currents.

Self-inhibition and Gating Analyses—To induce self-inhibition of ENaC activity by external Na^+ ions, bath solution was switched from a low Na^+ (1 mM Na^+ ions + 95 mM NMDG) to regular ND-96 solution (96 mM Na^+ ions) with an SF-77B Perfusion Fast-Step System (Warner Instruments). Cells were held at −60 mV. Current and voltage levels were digitized as described previously (39). Based on a two-state model (open-close), the maximal current levels at the zero time point and gating rates were computed according to the equation,

$$I(t) = I^0_{\max}\frac{k_a + e^{-(k_a + k_i)\cdot t}k_i}{k_a + k_i} \quad \text{(Eq. 1)}$$

where $I(t)$ represents experimental data for current, $I^0_{\max}$ is the maximal channel activity at the zero time point, k_a and k_i are activation and inactivation rates, respectively, and t is recording time.

Self-inhibition was divided into two phases: fast and slow. The rate for each phase was calculated as follows.

$$\int \text{fast} = \frac{k_i}{k_a + k_i} \quad \text{(Eq. 2)}$$

$$\int \text{slow} = 1 - \frac{I_{\text{sus}}}{I^0_{\max}} \quad \text{(Eq. 3)}$$

Computation of Electrically Detectable Channel Density at Cell Surface—To compute electrically detectable channel density (N^e) at the plasma membrane, the following equation was applied,

$$N^e = \frac{I^0_{\max}/E_m}{r \cdot A} \quad \text{(Eq. 4)}$$

where E_m is transmembrane potential difference, r is the cell diameter, and A represents area.

Biotinylation and Western Blots—Biotinylation experiments were adapted from previous publications (34, 42), using 20–40 oocytes/group. In some experiments, oocytes were preincubated in either ND-96 solution or low sodium solution (1 mM NaCl, 96 mM NMDG). Oocytes were incubated in freshly prepared biotinylation buffer (1.5 mg/ml EZ-Link Sulfo-NHS-SS-Biotin (Pierce) in Dulbecco's PBS solution (Hyclone), pH 8.0) for 30 min with gentle agitation. The biotinylation reaction was stopped by washing the oocytes three times for 5 min each with quenching buffer (192 mM glycine and 25 mM Tris-Cl, pH 7.5). Subsequently, the oocytes were incubated in ND-96 solution or supplemented with 10 μg/ml tcuPA for 60 min or designated periods for time-dependent study. After washing the oocytes three times with ND-96 solution, treated cells were lysed by passing them through a 27-gauge needle in lysis buffer (500 mM NaCl, 5 mM EDTA, 50 mM Tris, 1% Triton X-100, 1% Igepal CA-630, pH 7.4) and supplemented with Complete Mini EDTA-free protease inhibitor mixture (Roche Applied Science) according to the manufacturer's instructions. The lysates were incubated in a shaker for 1 h and centrifuged at 16,000 × *g* for 15 min at 4 °C. Supernatants were transferred to 1.5-ml tubes (Eppendorf). Biotinylated proteins were precipitated with 50 μl of prewashed high capacity neutravidin-agarose resin (Pierce). After overnight incubation at 4 °C with overhead rotation, supernatants were removed, and beads were washed three times with lysis buffer. 50 μl of 2× SDS-PAGE sample buffer (Pierce) containing protease inhibitors was added to the beads. Samples were boiled for 5 min at 95 °C, centrifuged for 1 min, and loaded on a 7.5% SDS-polyacrylamide gel. To detect small peptides by anti-HA antibody, samples were run on a 16.5% Tris-Tricine gel (Bio-Rad). To detect γ ENaC proteins, the membrane blots were blocked in 5% blocking buffer (5% nonfat dry milk, Bio-Rad, in TBST) for 1 h at room temperature. Then both anti-V5 and anti-HA monoclonal antibodies were added to the samples (1:5,000 and 1:1,000 dilution, respectively). Horseradish peroxidase-labeled secondary antibodies (Jackson Immunoresearch) were used (1:10,000). Chemiluminescence signals were detected using ECL Plus (Millipore). The fragments created by furin cleavage from Arg-135 and Arg-138 to Arg-178 could not be detected due to loss of HA tag.

In Silico Prediction of Cleavage Sites—Specific cleavage sites for both uPA and tPA were confirmed with phage substrate libraries (43–47). The consensus motif in substrates for proteolytic cleavage by urokinase is GR ↓ (S>N/K/R)(A≫S) from P2 to P2′. These sequences were used as custom input for the SitePrediction server (48) to predict potential cleavage site specifically for uPA in the extracellular loop of human γ ENaC. Default settings were used for all parameters except cleavage position (= 2) and cleavage sequences. The predicted sites must meet these criteria: 1) the cleavage site is located at the ectodomain of ENaC; 2) the size of the predicted carboxyl-terminal protein is close to those observed in Western blots; 3) the P1 protein must be Arg; 4) average score is >1; and 5) specificity is >99%.

Structural Analysis of Interactions between uPA and γ ENaC—The three-dimensional uPA-cleaved sites from P3 to P2′ in human γ ENaC (TGR ↓ KR) was generated by using "Tools>Build and Edit Protein" in Discovery Studio Visualizer version 4.0 (Accelrys, San Diego, CA). The surface view of chicken ASIC1 (Protein Data Bank code 3HGC) was adapted from Sherwood *et al.* (49), which was originally proposed by the Gouaux group (50, 51). The three-dimensional structure of uPA (Protein Data Bank code 1W12) reported by Zeslawska *et al.* was adapted (52). Following removal of the ligand from uPA, docking of the cleavage site in ENaC to uPA was performed with Autodock Vina version 1.1.1 (Scripps Institute, San Diego, CA) in a Pyrx (version 0.85) environment (Scripps Institute). The top-ranking pose with minimal energy in the docking results was selected and saved as a Protein Data Bank file. Final presentation was accomplished with Discovery Studio Visualizer version 4.0 by inserting the selected docking pose of the cleavage sites into the catalytic triad of uPA protein. The docking structure of uPA and cleavage site was further energy-minimized by "clean geometry." The uPA-ENaC interactions between the enzymatic domain and cleavage sites were visualized by a "non-bond interaction monitor" for a ligand-receptor mode.

All results were presented as mean ± S.E. Dose-response curves were fitted to the Hill equation (53). ENaC activity is the difference of the total and amiloride-resistant current fractions. Association of ENaC currents and uPA activity was computed for Pearson correlation. One-way analysis of variance computation combined with the Bonferroni test was used to analyze the difference of the means for significance. A probability level of 0.05 or less was considered significant.

RESULTS

Strong Up-regulation of ENaC Activity by tcuPA but Not tPA—Fibrinolytic activity is depressed in injured organs (*e.g.* in acute lung injury and pleural effusion). These organ injuries are characterized by fluid accumulation in the luminal cavities, where ENaC is critical for fluid resolution (54–56). uPA and tPA initiate fibrinolysis by converting plasminogen to plasmin. Although it is known that plasmin also activates ENaC, it is unknown whether or not ENaC activity is affected by plasminogen activators. To examine the effects of uPA on ENaC activity, oocytes expressing human αβγ ENaC were incubated with tcuPA (10 μg/ml) in OR-2 medium for 12 h. Compared with the control (Fig. 1*A*), total inward current generated by positively charged Na^+ ion flow was markedly greater in oocytes preincubated with tcuPA (Fig. 1*B*). Amiloride-resistant current fraction that was not mediated by ENaC appeared unaltered, indicating specific effects of the plasminogen activator. In contrast, amiloride-sensitive (*AS*) currents (*i.e.* ENaC activity) increased significantly (Fig. 1*C*).

We analyzed the effect of tcuPA on ENaC activity. tcuPA stimulated ENaC activity in a dose-dependent manner. A linear relationship was seen between tcuPA concentration above 5 μg/ml (100 nM) and ENaC currents (Fig. 1*D*). Furthermore, we characterized the time course for the activation of ENaC function by tcuPA. ENaC activity was determined in oocytes incubated for up to 24 h. As shown in Fig. 1*E*, ENaC activity was quickly elevated at 2 h, followed by a slow increment, finally reaching maximal activity at 8 h post-treatment. The ENaC currents subsequently declined slightly but were still significantly greater than the control ($p < 0.05$) at 24 h. The uPA enzyme activity was 80 and 20% of the initial level, at 8 and 24 h, respectively (Fig. 1*E*). Insufficient enzyme, altered endocytosis of channel proteins, and time-dependent expression of exogenous ENaC channels may contribute to the slight decline of current level after the 8 h time point.

Surprisingly, neither sctPA nor tctPA at a dose of 10 μg/ml altered ENaC activity (Fig. 1*F*). Tenecteplase was tested next to determine whether exosite interactions contribute to a sharp difference in the effects of tPA and uPA on ENaC activity. Tenecteplase is a mutant variant (T103N/N117Q/K296A/H297A/R298A/R299A) of tPA, which has higher than WT tPA fibrin specificity, and almost 2 orders of magnitude lower affinity for PAI-1 due to the elimination of positive charges in the 37-loop (57–59). However, neither sctPA nor tctPA nor tenecteplase in doses as high as 25 μg/ml affected ENaC activity (Fig. 1*F*), whereas enzymatic amidolytic activity toward LMW substrates (Fig. 1*G*) and plasminogen-activating activity (not shown) remained intact. Our study hereby adds a novel endogenous target to the uPA substrate pool.

uPA·PAI-1 Inhibitory Complex Does Not Affect ENaC Activity—A serpin, PAI-1, is a major specific endogenous mechanism-based inhibitor of uPA and tPA. Unlike tcuPA, neither active PAI-1 alone nor preformed uPA·PAI-1 inhibitory complex (10 μg/ml) had any effect on ENaC activity (Fig. 2*A*). These data indicate a lack of contribution of endogenous plasminogen activators to ENaC activity and indicate that the catalytic site of tcuPA contributes to the enhancement of ENaC activity.

Stimulation of ENaC Correlates with uPA Enzymatic Activity—The two polypeptide chains of an uPA molecule (amino-terminal fragment (ATF) and protease domain) are connected by a single disulfide bond between two cysteine residues (Fig. 2*B*, *top inset*).

To evaluate the contribution of uPA catalytic and ATF domains to activation of ENaC, a catalytically inactive S195A (chymotrypsin numbering) tcuPA and three uPA domain-deletion mutants, Δkringle, ΔCPD, and ΔGFD uPA, were compared with WT tcuPA. Oocytes expressing ENaC cRNA cultured in medium without uPA or its mutants were used as a negative control (Fig. 2*B*). Whereas inactive S195A tcuPA did not elevate ENaC current, all three mutant variants, which include the catalytic domain and possess enzymatic activity, activated ENaC (Fig. 2*C*). Therefore, there is only minimal (if any) contribution of ATF to ENaC activation by uPA.

We repeated these experiments by incubating oocytes with both wild type and mutant tcuPA preparations that, except for the S195A mutant, have equivalent enzymatic activity (Fig. 2*D*). Consistent with the previous experiment, the S195A tcuPA (negative control) did not affect ENaC activity. The three domain deletion mutants enhanced ENaC to an extent similar to WT tcuPA. These data demonstrate that the amino-terminal fragment is not involved in the activation of ENaC by tcuPA. Moreover, the same level of enzymatic activity associated with both wild type and mutant tcuPA, instead of identical mass,

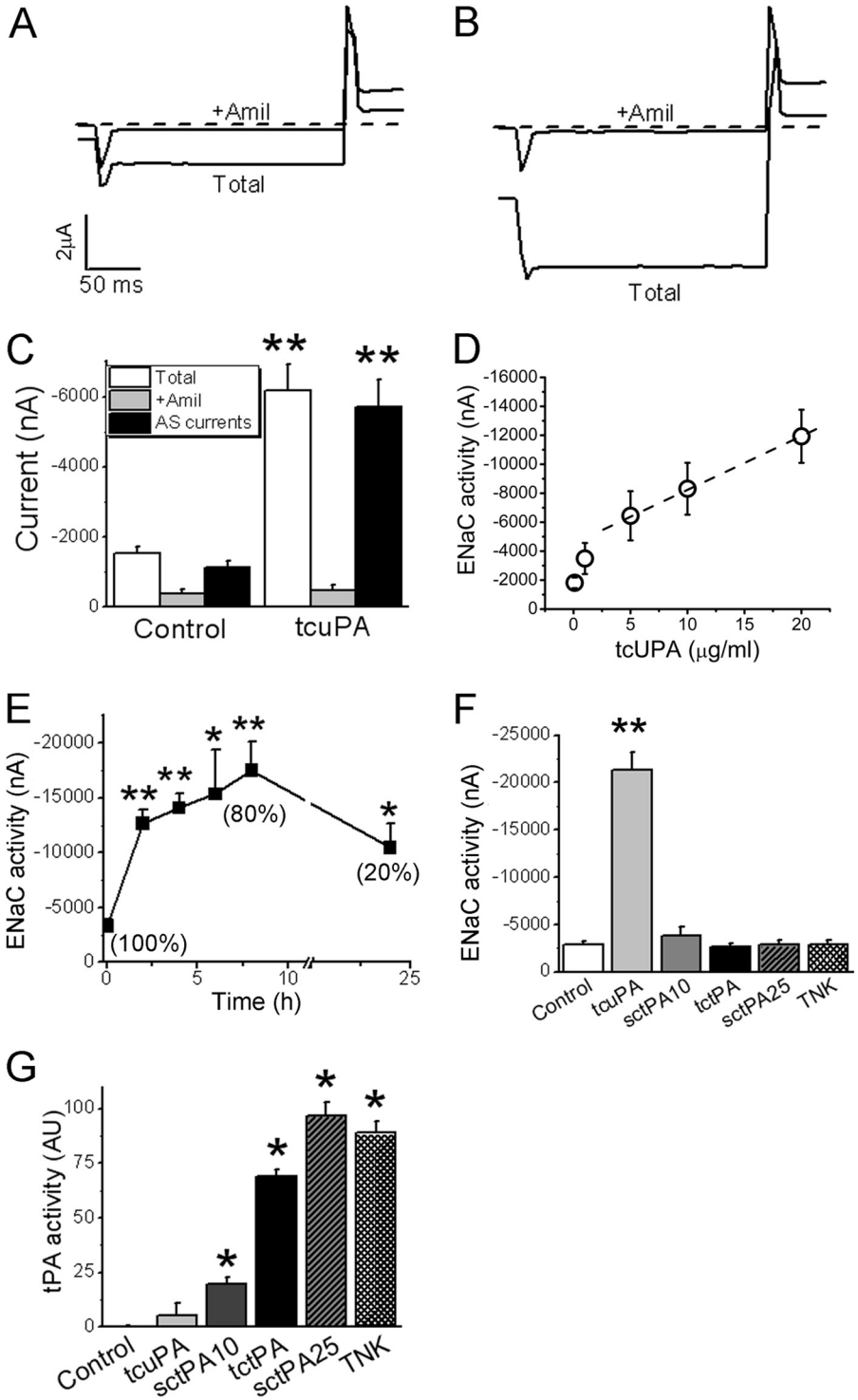

FIGURE 1. **tcuPA activates human $\alpha\beta\gamma$ ENaC activity.** *A* and *B*, representative inward current traces recorded in a control cell (*A*) and an oocyte incubated with tcuPA (10 μg/ml, 12 h) (*B*). The traces represent total sodium influx in the absence (*total*) and presence of amiloride (+*Amil*, 10 μM). *Broken lines*, zero current levels. Oocytes were held at −60 mV and sequentially stepped to −100 and +80 mV. *C*, average current levels for total, amiloride-resistant (+*Amil*), and amiloride-inhibitable (*ENaC activity*) fractions. The difference between the total and amiloride-insensitive currents reflects ENaC function. *AS*, amiloride-sensitive. $n = 25$; *, $p < 0.05$; **, $p < 0.01$ when compared with control oocytes. *D*, dose-effect relationship. Cells were incubated with tcuPA for 12 h. $n = 16$. *E*, time dependence of tcuPA-mediated activation of ENaC function. uPA activities at 0, 8, and 24 h are included in *parentheses*. $n = 14$; *, $p < 0.05$; **, $p < 0.01$ compared with the initial values at time 0. *F*, tPA does not alter ENaC activity. Shown are current levels in oocytes preincubated with 10 μg/ml tcuPA, 10 μg/ml single-chain tPA (*sctPA10*), 25 μg/ml tctPA, 25 μg/ml sctPA (*sctPA25*), and TNK. Control was cells in the absence of PA, and positive control was cells incubated with tcuPA. $n = 21$; **, $p < 0.01$. *G*, corresponding tPA activity in the culture medium. *, $p < 0.05$ *versus* control medium without plasminogen activators. *Error bars*, S.E.

determined the amplitude of ENaC currents. These results suggested a possible correlation between activated ENaC current levels and uPA enzyme activity.

We pooled experimental paired data for WT and mutated uPA as well as tPA constructs to compute the Pearson correlation. A correlation co-efficient of 0.93 was derived with a p

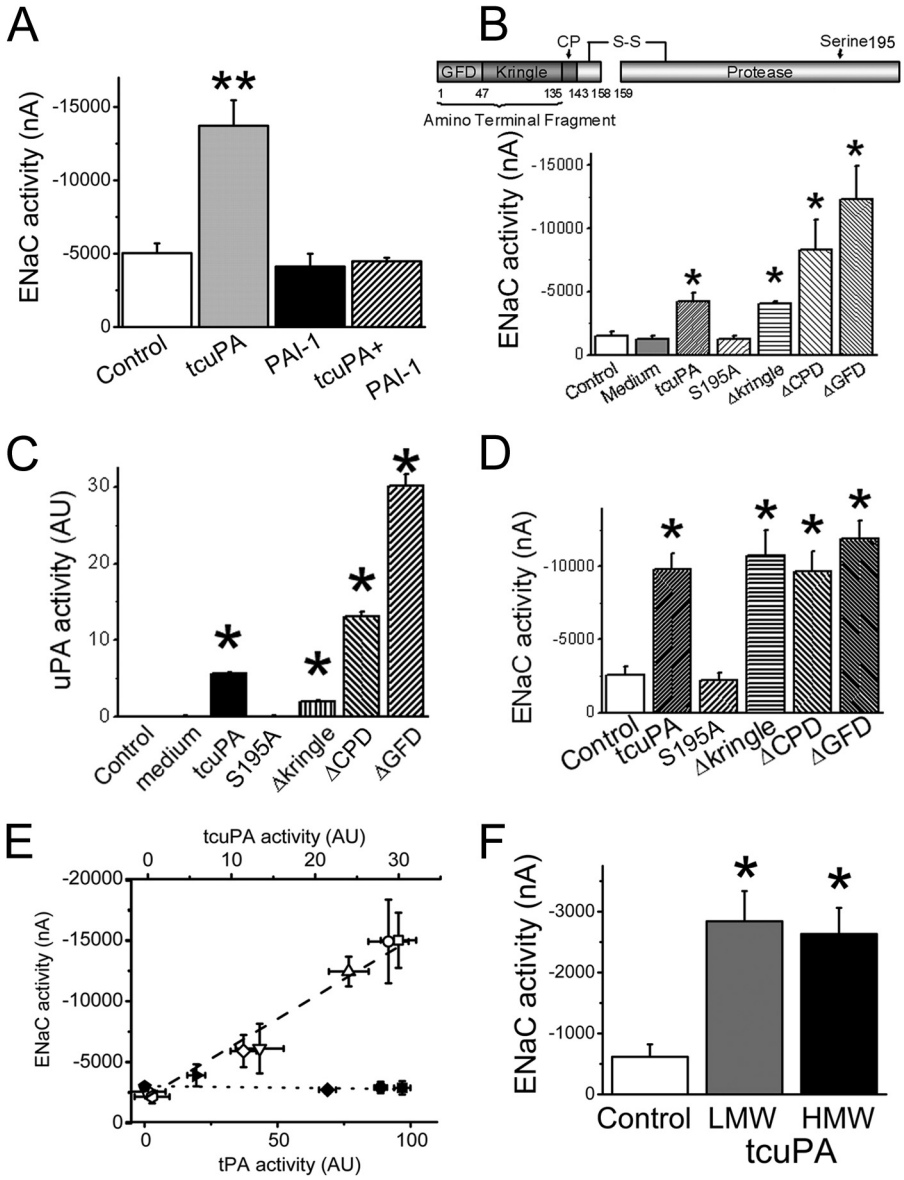

FIGURE 2. **Catalytic domain is required for the specific activation of ENaC by urokinase.** *A*, specificity of tcuPA-mediated regulation of ENaC activity. Enzymatic inhibition of tcuPA with PAI-1 prevents the activation of ENaC by tcuPA. Oocytes were incubated with tcuPA (10 μg/ml), PAI-1 (10 μg/ml), and their complexes (*tcuPA + PAI-1*) for 12 h. $n = 18$; **, $p < 0.01$ when compared with control oocytes. *B*, identification of critical domains in urokinase. *Top inset*, schematic linear structure of a tcuPA molecule. Two fragments of single-chain uPA are bridged by a disulfide bond. ATF is made up of GFD, kringle domain, and CPD. The catalytic site, serine 195, is located in the protease domain. Shown is ENaC activity in oocytes incubated with WT, catalytic site mutant (S195A tcuPA, chymotrypsin numbering), and three ATF-truncated tcuPA mutants Δkringle, ΔCPD, and ΔGFD. $n = 9$–17; *, $p < 0.05$ *versus* controls. *C*, corresponding uPA activity in culture medium. *D*, activation of ENaC by tcuPA and mutants possessing identical catalytic activity. *, $p < 0.05$ compared with controls; $n = 17$. *E*, correlation between ENaC and plasminogen activator activity. *Open symbols*, tcuPA; from *left* to *right*, control, S195A, Δkringle, LMW, HMW, ΔGFD, and ΔCPD. *Closed symbols*, tPA; from *left* to *right*, control, sctPA (10 μg/ml), tctPA, sctPA (25 μg/ml), and TNK. Pearson's correlation constant was 0.93; $p < 0.001$; $n = 12$. *F*, equivalent activation of ENaC by LMW and HMW tcuPA. *, $p < 0.05$; $n = 14$. *Error bars*, S.E.

value of 3.5E−6 between tcuPA and ENaC activity (Fig. 2*E*, *open symbols*). In sharp contrast, tPA enzyme activity showed no correlation with ENaC function (Fig. 2*E*, *closed symbols*).

uPA Receptor Does Not Mediate the Activation of ENaC by uPA—uPA, but not tPA, binds to uPA receptors (uPAR). Given that LMW uPA does not bind to uPAR but is still proteolytically active, we compared the effects of both HMW and LMW uPA on ENaC activity. As shown in Fig. 2*E*, both HMW and LMW tcuPA activate ENaC with comparable efficacy, suggesting that uPAR is not required for uPA to activate ENaC. To corroborate these observations, we compared the stimulatory effects of these two enzymes with identical activity. ENaC activity was activated to a similar extent by both LMW and HMW tcuPA (Fig. 2*F*). Taken together, it is unlikely that uPAR could affect this process unless it was situated in close proximity to the cleavage site to decrease the entropic barrier of the reaction.

uPA Strengthens the Open Conformation of ENaC—A two-state model (closed-open) has been proposed to analyze the gating kinetics of ENaC channels (60). We postulated that tcuPA opens closed channels and facilitates maintenance of activated ENaC in the open state. To analyze this possibility, gating kinetics were computed by measuring self-inhibition of external Na^+ ions (Fig. 3*A*). In addition to stable channel activity (reflected by sustained current level), the maximal channel

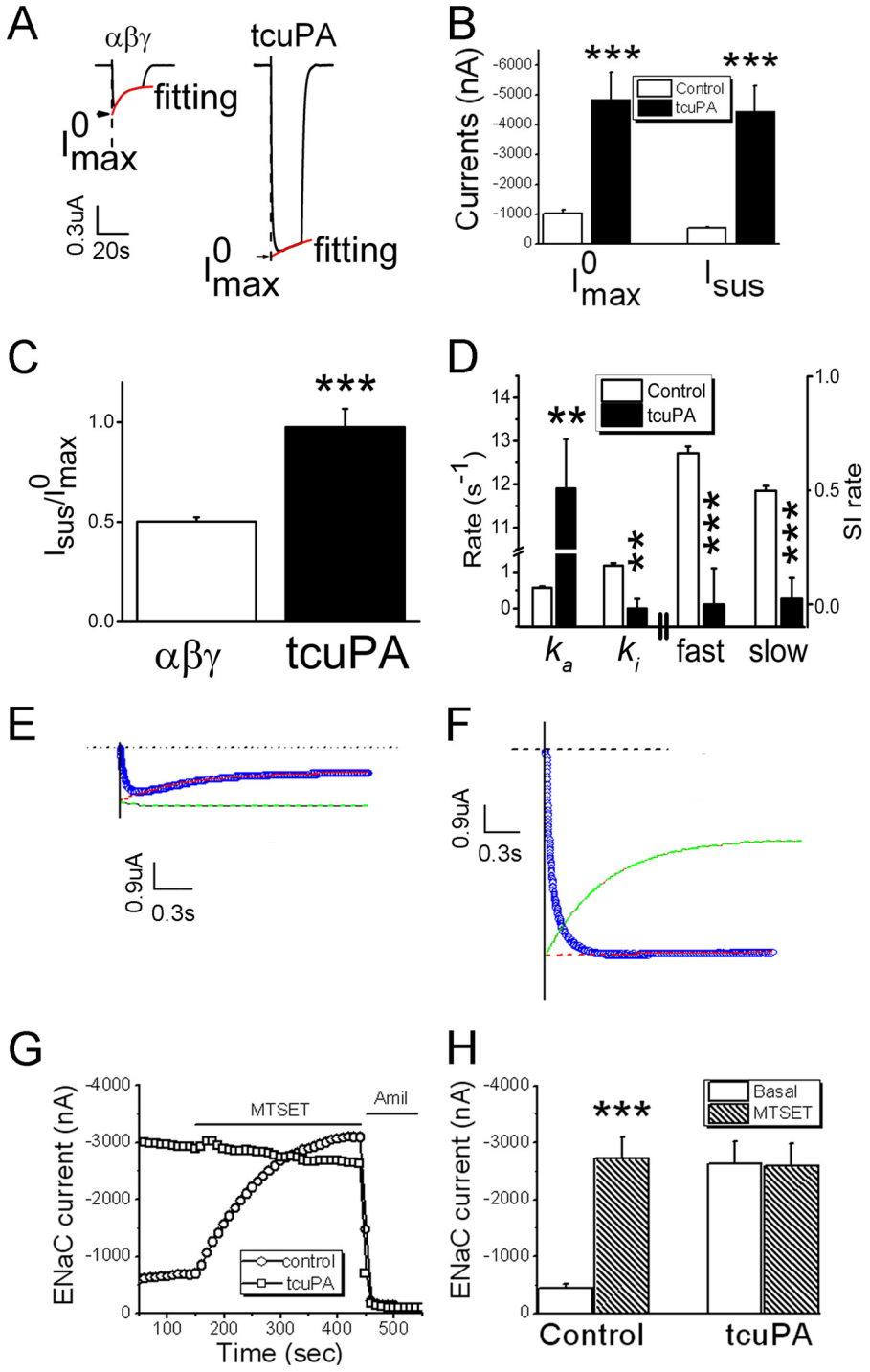

FIGURE 3. **uPA increases electrically detectable channel number and opening kinetics.** *A*, external Na^+ self-inhibition. Shown are representative traces for control ($\alpha\beta\gamma$) and tcuPA-treated cells. The maximal current level (I^0_{max}) at the zero time point (illustrated with *vertical broken lines*) and suspended amplitude (I_{sus}) were computed by fitting the climbing branch (*red lines*). See "Experimental Procedures" for details. *B*, average computed maximal suspended activation of ENaC by tcuPA. ***, $p < 0.001$ compared with controls; $n = 12$. *C*, ratio of stable and maximal current magnitudes. ***, $p < 0.001$ compared with controls; $n = 12$. *D*, gating kinetics of ENaC channels. *Left*, K_a (activation rate) and K_i (inactivation rate). *Right*, fast and slow phases of self-inhibition (*SI*) process. **, $p < 0.01$; ***, $p < 0.001$ compared with controls. $n = 12$. *E* and *F*, simulation of maximal opening level for control (*E*) and tcuPA-treated cell (*F*). *Top*, *broken black lines* indicate background current level at 0 mM external Na^+ ions. *Symbols* in *blue*, experimental data. *Red broken lines* were created by fitting raw data points with Equation 1. *Green lines*, simulation levels for maximal level in the absence of self-inhibition in control cells (*E*) and pseudo-self-inhibition in the presence of self-inhibition. *G*, effects of tcuPA on $\alpha\beta$S520Cγ ENaC activity. Traces showing application of MTSET and amiloride (*Amil*, 10 μM) to tcuPA-incubated and control cells. *H*, comparison of ENaC activity before and after the addition of MTSET. ***, $p < 0.001$ *versus* basal current level in the presence of MTSET. $n = 19$. *Error bars*, S.E.

activity (measured as peak current) was significantly greater than in control cells (Fig. 3*B*). The ratio of sustained over maximal current levels is ~0.5 for ENaC channels in control cells, which is consistent with previous observations (39, 61, 62). By comparison, the value was close to 1.0 following exposure to tcuPA (Fig. 3*C*). These results suggest that self-inhibition is

diminished by tcuPA. There are two components of self-inhibition: a fast phase followed by a slow phase (Fig. 3*A*). The rate of activation process after incubation with tcuPA was almost an order of magnitude faster than that for untreated cells (1.17 and 11.9 s^{-1} for control and tcuPA treatment, respectively; Fig. 3*D*, *left*). Moreover, treatment with tcuPA completely eliminated inactivation (the inactivation rate was reduced by tcuPA from 0.56 to 0.0 s^{-1}). In addition, even with switched gating rates between control and tcuPA-treated cells, the simulated maximal current level at the full open state for controls was still much lower than the sustained current magnitude of tcuPA-challenged cells (Fig. 3, *E* and *F*). These observations could not simply be explained by full opening of activated channels in untreated cells. On the other hand, irreversibility of the effect of tcuPA on ENaC gates most likely reflects cleavage of ENaC by tcuPA, resulting in transition to the "open" conformation of the channel.

Channel activity recorded in whole-cell mode is the product of single-channel activity and unitary conductance. The latter was not altered during self-inhibition, as has been demonstrated by self-inhibition mutations (39, 62). Single-channel activity is the product of open probability and electrically detectable channel density. The simulation leads us to ask whether there is a potential increment in functional channel density. The functional channel density was computed using Equation 4 (see "Experimental Procedures." Our calculation found that the channel number that could be detected per unit area was 410 channels/μm^2 post-uPA exposure. This is 5-fold greater than that in control cells (82 channels/μm^2). It appears that uPA increases functional channel density at the plasma membrane. This is supported by studies of other serine proteases (63–65).

MTSET is a thiol-modifying reagent that activates $\alpha\beta$S520Cγ channels almost completely as evidenced by an open probability of nearly 1.0 (66). If uPA activates ENaC activity via an increment in opening time, with a mechanism similar to that mediated by MTSET, then uPA should not alter ENaC whole-cell currents in MTSET-pretreated cells expressing $\alpha\beta$S520Cγ channels. Our results indicate that although MTSET does increase channel activity in untreated cells to a level similar to that in uPA-incubated cells (Fig. 3, *G* and *H*), it does not affect uPA-activated ENaC activity. These observations provide evidence for uPA maintenance of ENaC channels in the fully open state, with a resultant effect equivalent to that of MTSET. uPA may proteolytically cleave ENaC, a common mechanistic translational modification of ENaC proteins, as demonstrated by numerous proteases (63–65). These observations prompted us to address the idea that tcuPA selectively cleaves ENaC proteins.

γ ENaC Is Cleaved by tcuPA—To identify what subunits are cleaved by tcuPA, a well established measurement of amiloride-sensitive sodium ion flow was applied (Fig. 4*A*). We expressed α alone, $\alpha + \beta$, and $\alpha + \gamma$ in oocytes. tcuPA slightly stimulated current level in cells expressing α ENaC alone ($p > 0.05$). The change in cells co-expressing $\alpha + \beta$ ENaC subunits was not significant. In sharp contrast, the activity of channels composed of $\alpha + \gamma$ ENaC subunits was increased ~3-fold ($p < 0.05$). These results indicate that the γ subunit could be a target for tcuPA.

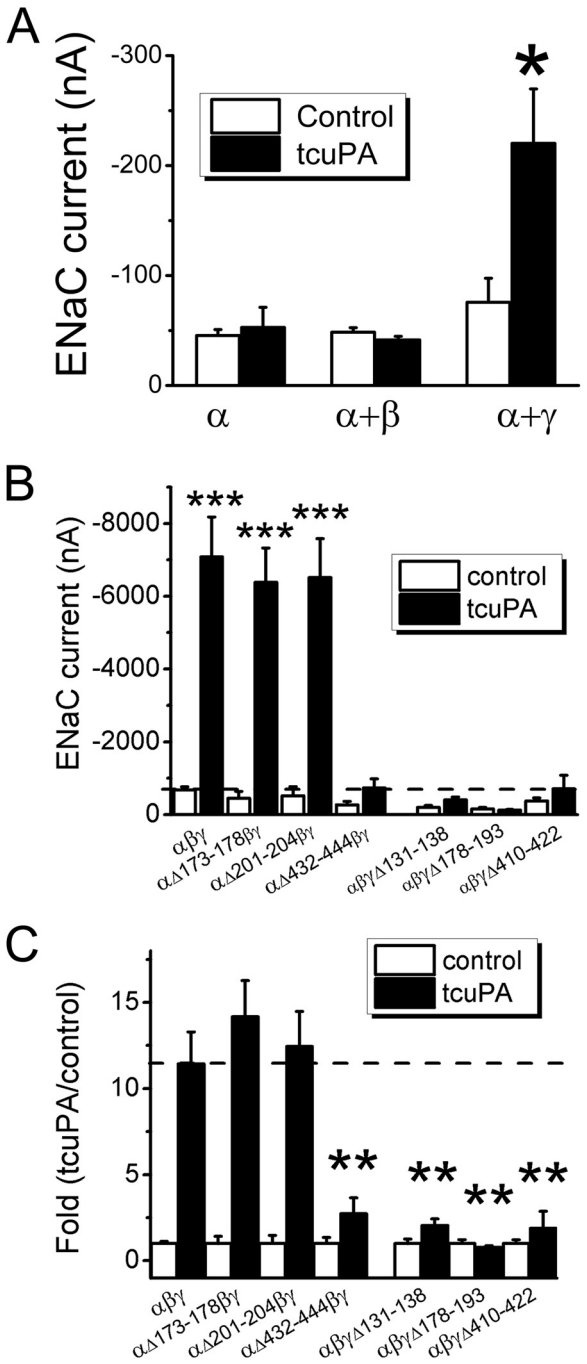

FIGURE 4. **Identification of tcuPA-regulated domains in ENaC subunits.** *A*, γ subunit is required. tcuPA was incubated with cells expressing α ENaC alone (α), co-expressing α and β subunits ($\alpha + \beta$), and co-expressing α and γ subunits ($\alpha + \gamma$). *, $p < 0.05$. $n = 6–13$. *B*, effects of tcuPA on deletion mutants of the putative cleavage domains. The ratio of current level in the presence and absence of tcuPA was computed to compare the -fold increase in currents. **, $p < 0.01$; $n = 8–24$. *Error bars*, S.E.

As proposed and confirmed by several groups, there are three putative cleavage domains (67–70). To narrow down the search range for uPA cleavage sites, we constructed three deletion mutants for both α ($\alpha\Delta$131–138, $\alpha\Delta$178–193, and $\alpha\Delta$410–422) and γ ENaC subunits ($\gamma\Delta$131–138, $\gamma\Delta$178–193, and $\gamma\Delta$410–422) and expressed them in oocytes. We reasoned that after removal of tcuPA cleavage sites from these ENaC subunits, channel activity associated with these cleavage site-miss-

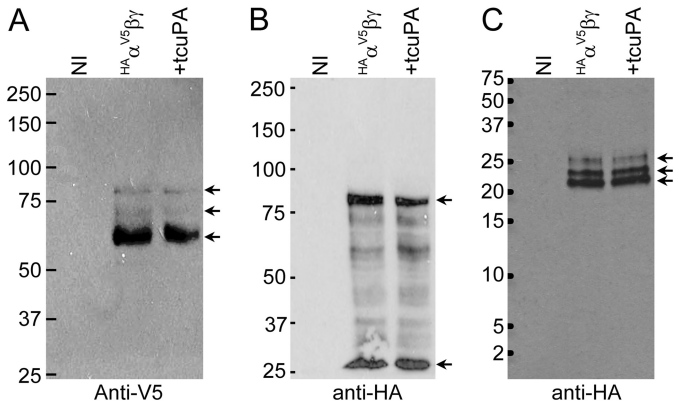

FIGURE 5. **Proteolytic cleavage of α ENaC by tcuPA.** *A*, detection of $^{HA}\alpha^{V5}$ ENaC with anti-V5 monoclonal antibody. From *left* to *right*, lanes were loaded with biotinylated plasma membrane proteins of noninjected oocytes (*NI*), cells coexpressing $^{HA}\alpha^{V5}$, *β*, and γ ENaC subunits, and those treated with tcuPA. *Arrowheads*, signals recognized by the antibodies. *B*, Western blot probed with anti-HA antibody. *C*, analysis of short amino-terminal peptides using 16.5% Tris-Tricine protein gel. These experiments were repeated at least three times with similar results. Relative mobility of the standard mixture of proteins is shown to the *left*.

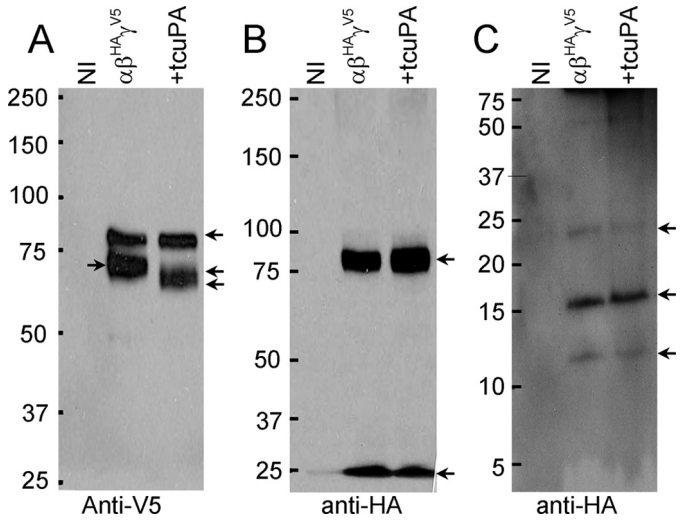

FIGURE 6. **Cleavage of γ ENaC by tcuPA.** *A*, tcuPA cleaves γ ENaC. Plasma membrane proteins with the carboxyl-terminal tail were detected with anti-V5 monoclonal antibody after running on a 7.5% SDS-polyacrylamide gel. *B* and *C*, Western blots probed with anti-HA antibody to detect membrane proteins on 7.5% SDS-polyacrylamide gels (*B*) and 16.5% Tris-Tricine gels (*C*). These experiments were repeated at least three times with similar results. Relative mobility of the standard mixture of proteins is shown to the *left*.

ing mutants should not be altered by tcuPA. Intriguingly, four mutants, one of α ENaC and all three deletion mutants of γ ENaC subunit, did not respond to tcuPA (Fig. 4*B*). Because the current levels between each construct vary before application of uPA, as shown by the *open bars* in Fig. 4*B*, we computed -fold increase in the ENaC activity and plotted normalized data in Fig. 4*C*. These results suggest that a uPA-specific cleavage motif may be located within these four deleted ectodomains.

We then constructed V5 (carboxyl-terminal) and HA (amino-terminal) tagged α ($^{HA}\alpha^{V5}$) and γ ENaC ($^{HA}\gamma^{V5}$) to examine tcuPA-mediated proteolysis combining biotinylation and Western blots. As shown in Fig. 5*A*, three bands of α ENaC were recognized by anti-V5 monoclonal antibody. One small fragment at 25 kDa in addition to a full-length signal was identified by anti-HA antibody (Fig. 5*B*). Furthermore, three small bands could be visualized on 16.5% Tris-Tricine gels by anti-HA antibody. The same signal patterns of α ENaC were found in the absence and presence of tcuPA, either with anti-carboxyl terminus (-COOH) or anti-amino terminus (-NH_2) antibody. These results exclude the cleavage of α ENaC proteins by tcuPA, further substantiating the functional results in Fig. 4.

In strict contrast to α ENaC, two peptides of γ ENaC were visualized by anti-V5 antibody for full-length proteins (86 kDa) and endogenous furin-cleaved carboxyl-terminal fragments (70 kDa) in the absence of tcuPA (Fig. 6*A*). By comparison, in the presence of tcuPA, carboxyl-terminal fragments with a smaller size (65 kDa) than that of furin-cut fragments along with the full-length proteins were seen. Strikingly different from anti-V5 antibody-recognized signals, proteins detected by anti-HA monoclonal antibody displayed a similar pattern, either on 7.5% SDS-polyacrylamide gels (Fig. 6*B*) or 16.5% Tris-Tricine gels (Fig. 6*C*). The same pattern for ENaC expression was found between controls and tcuPA-treated groups, indicating that the furin sites may precede the cleavage domains for tcuPA. Thus, the subsequent Western blots were done with anti-V5 antibody to examine uPA-cleaved carboxyl-terminal peptides as well as full-length translations.

Proteolysis of Deletion Mutants Missing Consensus Motifs for Proteolysis—Given the fact that tcuPA could not stimulate channel activity associated with all three deletion mutants of γ ENaC (Fig. 4*B*), cleavage of these three deletion mutants by tcuPA was examined with the full-length γ ENaC as control (Fig. 7*A*). The furin-cleaved band was very faint for αβγΔ131–138 channels (Fig. 7*B*), supportive of previous reports that furin sites are located within the first putative proteolysis tract (67–70). tcuPA apparently could not cleave ENaC proteins of furin site-defective αβγΔ131–138 channels. As to the cells expressing αβγΔ178–193 channels (Fig. 7*C*), the same pattern of ENaC proteins was seen in the presence and absence of tcuPA. Removal of the third putative domain (Δ410–422) appeared to alter the cleavage efficacy of uPA on furin-cut proteins (Fig. 7*D*). Compared with WT channels (Figs. 6*A* and 7A), the uPA-cleaved band is weaker. Based on the identical migration of cleaved bands associated with αβγΔ178–193 channels in the absence and presence of tcuPA, we postulated that uPA-specific cleavage sites could be within the second putative domain (from amino acid 178 to 193).

Identification of uPA-specific Cleavage Sites in γ ENaC—Several serine proteases, including prostasin ($RKRK^{178}$), human neutrophil elastase (Val-182, Val-193), and plasmin (Lys-189) trimmed the second consensus proteolysis motif (67–70). It is conceivable that all of these residues are targeted by tcuPA (Fig. 8, *top inset*). This is at least the scenario for plasmin to cleave human γ ENaC (34). Indeed, the plasmin cleavage site composed of five amino acid residues for prostasin and one for murine plasmin ($^{178}RKRK^{181}$ + Lys-189), when substituted with alanine (termed γ5A, $^{178}AAAA^{181}$ + Ala-189) was not stimulated by tcuPA even after 24 h (Fig. 8*A*). Moreover, the tcuPA-cleaved band disappeared compared with that of wild type channels (Fig. 8*C*).

A series of classic studies on the specificity of uPA substrates revealed a consensus cleavage motif, GR ↓ (S>N/K/R)(A≫S)

from P2 to P2′ (43, 44). We further combined *in silico* prediction and immunoblotting assays to narrow down the cleavage site. Using the SitePrediction server (48), only one hit was predicted: ^{177}GR ↓ KR within the ectodomain of human γ ENaC with a specificity above 99%. In strict contrast, no specific cleavage sites in human γ ENaC were found for tPA with its cleavage motif, (F/Y/R)GR ↓ R(A/G) from P3 to P2′ (data not shown). In addition, there are no predicted cleavage sites in human α, β, and δ ENaC proteins for uPA to meet the prediction criteria (see "Experimental Procedures"). Does uPA cut γ ENaC proteins into two fragments between Arg-178 and Lys-179? We validated this prediction combining mutagenesis, functional measurements, biotinylation, and immunoblotting assays. Neither γR178A nor γK179A could be significantly activated by tcuPA in 24 h (Fig. 8*B*). We anticipated that the uPA-cleaved band of R178A and K179A should migrate slower than that of wild type if any. Intriguingly, this is the case for K179M, and probably K179A but not R178A. This phenomenon is consistent with the functional data shown in Fig. 8*B*. Combined with the blot for the deletion mutant in Fig. 7*C*, we believe that amino acid residues from P2 to P2′ (^{177}GRKR^{180}) coordinately interact with uPA to serve as a catalytic triad. Of them, both

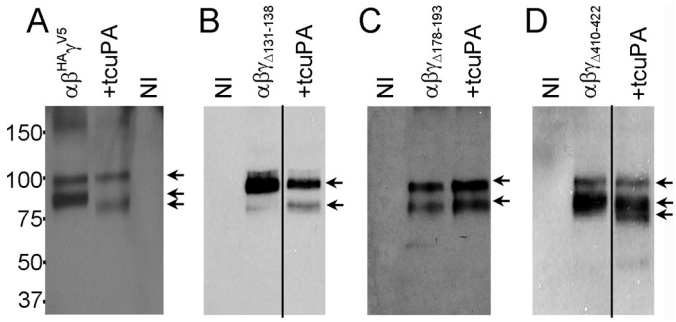

FIGURE 7. **Proteolysis of γ ENaC putative cleavage domain deletion mutants by tcuPA.** *Blots A–D* represent wild type, deletion of 131–138 (Δ131–138), deletion of 178–193 (Δ178–193), and deletion of 410–422 (Δ410–422), respectively. The *lanes* in each blot (from *left* to *right*) contain lysates from noninjected cells (*NI*), wild type and mutated γ ENaC, and tcuPA-treated cells. These experiments were repeated at least three times with similar results. Relative mobility of the standard mixture of proteins is shown to the *left*.

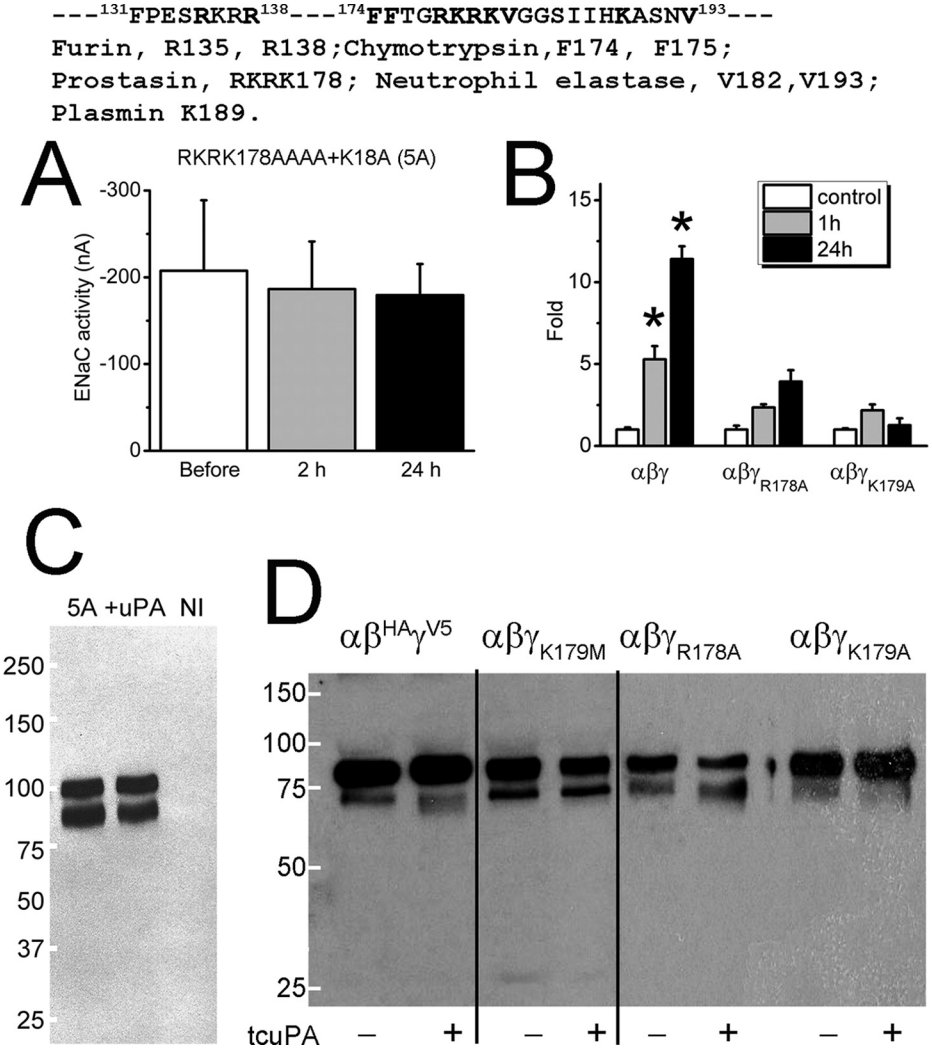

FIGURE 8. **Identification of cleavage sites for tcuPA in the γ subunit.** Identified cleavage sites for furin, chymotrypsin, prostasin, elastase, and plasmin are listed at the *top*. *A*, effects of tcuPA on γ5A mutant (*RKRK178AAAA + K189A*). Shown is the ENaC activity in the absence and presence of tcuPA 2 and 24 h postaddition. $n = 24$. *B*, effects of tcuPA on R178A and K179A mutants. $n = 22$; *, $p < 0.05$ *versus* controls prior to application of tcuPA. *C*, Western blots for cleavage of γ5A by tcuPA. *NI*, noninjected eggs. *D*, cleavage of Arg-178 and Lys-179 mutants by tcuPA. This blot represents four experiments with similar results. Relative mobility of the standard mixture of proteins is shown to the *left*. *Error bars*, S.E.

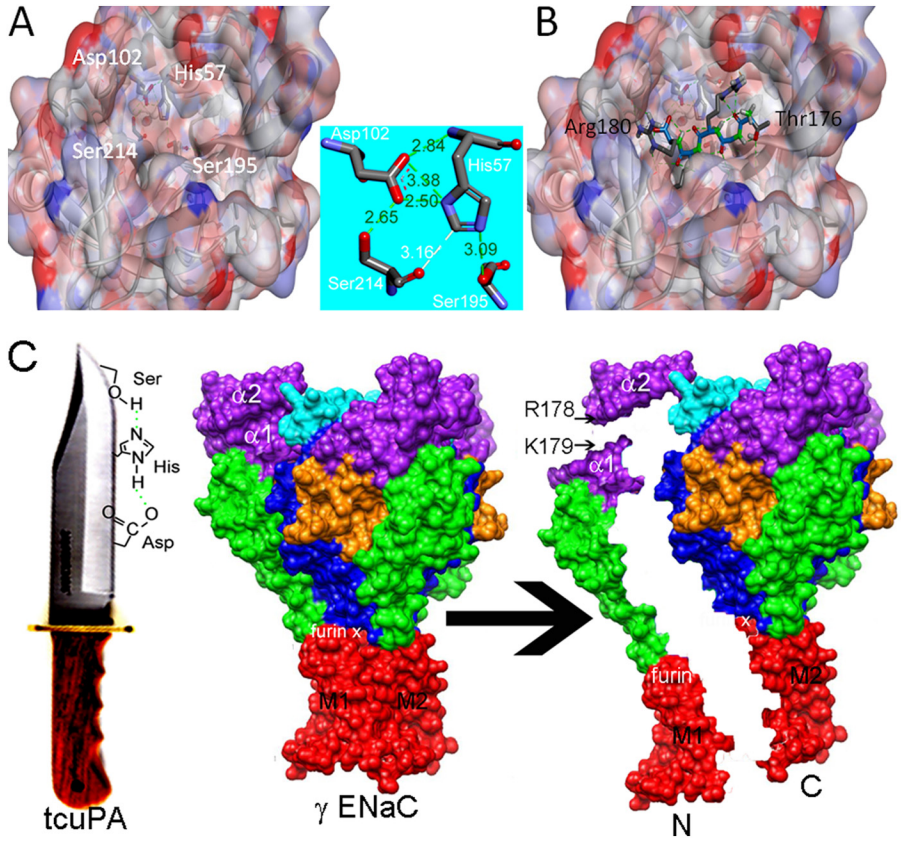

FIGURE 9. **Structural interactions between uPA and human γ ENaC.** *A*, *surface view* of the catalytic triad of uPA (Protein Data Bank code 1W12) (52). The triad residues (Asp-102, His-57, and Ser-195) along with His-99 line the back of the enzyme active center. *Inset*, measures of hydrogen (*green* and *white dashed lines*) bonds among amino acid residues composed of the catalytic triad. *B*, docking of the cleavage site (P3–P2′) of γ ENaC to the enzyme active pore of uPA. *C*, uPA-induced cleavage of the γ ENaC. Arg-178 and Lys-179 are located between the α1 and α2 domains. Domain coloration is as follows: transmembrane domains 1 and 2 (*TM1* and *TM2*) (*red*), wrist (*red*), palm (*blue*), knuckle (*cyan*), finger (*purple*), thumb (*green*), and β (*orange*).

Arg-178 and Lys-179 amino acid residues are critical for uPA-mediated proteolysis.

Structural Interactions between Catalytic Sites of uPA and Cleavage Sites of γ ENaC—The cleavage sites in the γ ENaC (Arg-178 and Lys-179) are located between α1 and α2 of the finger, a hypervariate region. The confident docking of the uPA-specific cleavage site into the enzyme active center of uPA substantiates their protein-protein interactions (Fig. 9, *A* and *B*). A network of hydrogen bonds within the catalytic triad of uPA was visualized (*inset between A* and *B* of Fig. 9). Importantly, hydrogen bonding pairs are detected between His-57 (uPA) and Lys-179/Arg-180 (ENaC) and Ser-195 (uPA) and Arg-178/Lys-179 (ENaC). In addition, Thr-176 (ENaC) interacts with His-99 (uPA). Arg-178 (ENaC) protrudes down into a deep cavity and interacts with other residues in the bottom of the cavity (data not shown). Proteolysis of ENaC by uPA could be divided into two steps: acylation and deacylation (71). As shown in Fig. 9*C*, Ser-195 of uPA, together with His and Asp, serves as a nucleophilic "edge" to separate Arg-178 from Lys-179 of γ ENaC, generating two fragments: the carboxyl-terminal peptide and the amino-terminal peptide.

DISCUSSION

Fibrinolytic activity is depressed in edematous pulmonary injury due to elevated PAI-1 level and depressed uPA. We set out to examine the effects of tPA and urokinase on ENaC, a key pathway for edema fluid resolution. Our results demonstrate that uPA, a sole contributor of fibrinolysis in the airway and alveolar sacs, but not tPA, activates heterologously expressed human αβγ ENaC function in a time- and dose-dependent manner. The specificity of its stimulatory action is supported by the following lines of evidence. uPA·PAI-1 complexes could not alter ENaC activity. The uPA-mediated activation of ENaC can be eliminated by mutating its catalytic domain (Ser-195) within the protease peptide. uPA directly activates ENaC through an increment in opening time and in functional channel density. γ ENaC proteins are proteolytically cleaved by uPA into two fragments following hydrolysis of ^{177}GR ↓ KRK^{181}, a motif possessing uPA substrate specificity. Urokinase primarily cleaves furin-trimmed proteins. Our results identified critical domains, the cutting edge in urokinase and the cleavage motif in ENaC through which urokinase up-regulates epithelial sodium transport.

The striking difference between the effects of uPA and tPA on ENaC activity (Fig. 2*E*) could reflect different mechanisms of fine regulation of fluid absorption in the thoracic cavity and in circulation. tPA is not expressed in alveolar or pleural spaces but is predominantly expressed in capillary endothelial cells and circulates in the blood stream. Both tPA and uPA could activate plasminogen. However, only uPA is able to bind to uPAR. Our results exclude uPAR as a mediator between ENaC

and uPA. The substrate pool for tPA is much smaller than that for uPA. Moreover, *in silico* prediction for cleavage sites and protein docking analysis reveal a difference between those two types of plasminogen activators. Parallel analysis of tPA enzymatic activity in culture and experimental medium rules out the possibility that tPA preparations are not active. We herein demonstrate that γ ENaC proteins contain a peptide serving as uPA-specific substrate.

Our functional data confirm that uPA increases the opening time of ENaC channels and the channel density detected by electrical approaches. The augmentation of functional channel density could be due to activation of nearly "silent" channels. We could not exclude potential accumulation of channel proteins at the plasma membrane. This might result from facilitated exocytosis and weakened endocytosis. Based on the enzymatic activity of uPA, the time-dependent decrease in the ENaC current (Fig. 1*E*) could reflect faster internalization of the "opening" ENaC, when compared with delivery of freshly expressed uncleaved ENaC to the plasma membrane.

It is well accepted that external serine proteases can only access furin-cleaved ENaC proteins. Our data show that uPA, a trypsin-like serine protease, is unable to cleave the proteins and to increase the channel activity of the deletion mutant lacking furin sites. Our data support the notion that external protease could not cleave full-length translations of ENaC channels. Additionally, we tried to examine the cleavage of furin-cut proteins by tcuPA. We incubated oocytes in a low sodium medium (1 mM NaCl) to eliminate full-length proteins, a strategy successfully used in HEK293T cells and oocytes (34, 72). Unfortunately, the full-length proteins could not be eliminated. There was no difference in the protein signals for both full-length and furin-cut fragments between controls and cells exposed to low sodium medium.

Divergent specificity of substrates between uPA and tPA may explain why uPA but not tPA cleaves human γ ENaC. As predicted by the SitePrediction server, there is only one cleavage domain specific for uPA in human γ ENaC. These *in silico* predictions are experimentally confirmed with both functional and immunochemical approaches. Although the P2P1 sequence for both tPA and uPA is Arg-Lys, the hydrophilic amino acid residues at P3 are required for tPA to access its cleavage site (44), whereas it is tyrosine at the 176th amino acid residue. Additionally, P1 and P2 positions of the tcuPA cleavage motif (^{176}TGR ↓ KR^{180}) are not favorable for tPA (R(A/G)).

Three putative domains for proteolysis in α and γ subunits have been proposed, and these predictions have been supported by accumulating experimental evidence across various species (67–70). In addition, β ENaC could be cleaved by channel-activating protease 2, as shown by Stutts and co-workers (73). It is unlikely that α and β ENaC subunits are cleaved by uPA. We did not find cleaved bands for α ENaC. Although β ENaC was not analyzed in this study, both functional and immunoblotting assays of the cleavage sites in γ ENaC for uPA exclude the potential involvement of additional domains/subunits.

The relationship between activated channels and furin cleavage is unknown. Determination of whether full-length proteins are nearly "silent" functionally or furin-cut channels are all open requires further experimental evidence. Although the channel activity of MTSET-treated αβS520Cγ channels could not be further augmented by external proteases, including uPA, the channel activity associated with furin-cut proteins in H441 cells was still significantly activated by the subsequent addition of trypsin.

Under our experimental conditions, furin-cut γ ENaC fraction counts for more than 50% of the total membrane proteins. Intracellular proteolysis of ENaC proteins by endogenous furin may favor subsequent cleavage by external uPA by exposing the specific domains to urokinase.

It has been reported that the PAI-1 level is extremely elevated in edema fluid, accompanied by a concurrent elimination of fibrinolytic activity (14, 16, 18, 74, 75). Several groups reported that edema fluid of infected lungs but not cardiogenic pulmonary edema inhibits ENaC activity (76–80), which supports our observations that uPA activates ENaC function. We recently demonstrated that uPA deficiency leads to reduced cleavage of mouse lung ENaC *in vivo* (81). In injured tissues, elevated PAI-1 would specifically bind to uPA to form plasminogen activator inhibitor·uPA complexes (82). Subsequently, the uPA·α-macroglobulin complexes should be unable to trap ENaC and serve as a trimer for ENaC molecules.

Both tPA (alteplase) and uPA (abbokinase) are broadly utilized in fibrinolytic therapy of pleural effusions, acute lung injury, acute respiratory distress syndrome, and airway injuries (83, 84). The novel regulatory mechanism of ENaC activity described here could potentially be used toward resolution of edema and pleural effusions during fibrinolytic therapy. Regarding the mechanisms of how tPA might regulate edema fluid resolution although it neither activates ENaC nor uPAR, we postulate that a tremendous dose of tPA may benefit edematous injury through reduction of free PAI-1 levels post-tPA·PAI-1 complex formation. tPA competitively binds to PAI-1 with a greater affinity than its urokinase counterpart.

uPA is able to form complexes with its specific inhibitors, PAI-1, PAI-2, and α_2-macroglobulin; uPA receptors (uPAR and plasminogen activator receptors); and plasmin and amiloride. The uPA activity depends on free moles of two-chain uPA in the presence of various binding proteins. Urokinase has been used clinically and preclinically for the last 3 decades. The bolus dose applied has been from 500 to 700,000 IU for empyema, breast abscesses, pulmonary fibrosis, asthma, and pleural injury (85–91). The physiological concentration in human bronchoalveolar lavage fluid is 0.129 ± 0.06 IU/ml (15), which tends to rise to the serum level (0.362 ± 90 μg/ml) in injured lungs (92). Under our experimental conditions, both the time course and dose-dependent studies show that uPA at this concentration fully activates ENaC up to 24 h (Fig. 1). The detectable uPA activity is ~4 AU. The dose below 10 μg/ml (600–1,000 IU/ml) would take several h to activate ENaC activity. It is hard to separate the contributions of proteolysis from exocytosis of channel proteins and to detect uPA enzymatic activity.

In summary, our results for the first time demonstrate that tcuPA, but not tPA, specifically activates human ENaC. The irreversible activation of ENaC by uPA is solely determined by urokinase enzymatic activity. Moreover, uPA releases self-inhibition of ENaC, increases the activation rate, activates "silent" channels, and catalyzes the γ subunit. Eventually, ENaC func-

tion is fully up-regulated by tcuPA. Our data may help to explain the differences in pharmaceutical efficiency and tissue dependence between tPA and uPA. In ENaC-expressing epithelial and mesothelial tissues (*e.g.* the airways, lungs, pleural cavity, kidney, and distal colon), it should be kept in mind that either endogenous or administered uPA may dehydrate the lumen through excessive activation of ENaC-mediated salt/fluid retention. uPA, as an ENaC activator, may be a potent pharmaceutical agent to mitigate lung edema and pleural effusion.

Acknowledgments—We thank Andrew Lee, Raul Molina, Deepa Bhattarai, Dr. Xue-Feng Su, Dr. Dr. Shaohu Sheng (University of Pittsburgh), Dr. Dongyun Han, and Dr. Steven Idell for superb technical support and thoughtful discussion.

Note Added in Proof—The version of this article that was published on January 2, 2015 as a Paper in Press contained errors in Figs. 6–8. Fig. 6 was omitted and replaced with a duplicate of Fig. 5 that was labeled Fig. 6. The *inset* of Fig. 8 showed a "C" instead of the correct amino acid, "G," at position 177 in the protein sequence of γ-ENaC. The Western blots in Figs. 7 and 8 were assembled from separate sections without lines indicating the borders between the sections. These errors have been corrected.

REFERENCES

1. Shetty, S., Padijnayayveetil, J., Tucker, T., Stankowska, D., and Idell, S. (2008) The fibrinolytic system and the regulation of lung epithelial cell proteolysis, signaling, and cellular viability. *Am. J. Physiol. Lung Cell Mol. Physiol.* **295,** L967–L975
2. Sisson, T. H., and Simon, R. H. (2007) The plasminogen activation system in lung disease. *Curr. Drug Targets* **8,** 1016–1029
3. Nishiuma, T., Sisson, T. H., Subbotina, N., and Simon, R. H. (2004) Localization of plasminogen activator activity within normal and injured lungs by *in situ* zymography. *Am. J. Respir. Cell Mol. Biol.* **31,** 552–558
4. Gross, T. J., Simon, R. H., and Sitrin, R. G. (1990) Expression of urokinase-type plasminogen activator by rat pulmonary alveolar epithelial cells. *Am. J. Respir. Cell Mol. Biol.* **3,** 449–456
5. Marshall, B. C., Sageser, D. S., Rao, N. V., Emi, M., and Hoidal, J. R. (1990) Alveolar epithelial cell plasminogen activator. Characterization and regulation. *J. Biol. Chem.* **265,** 8198–8204
6. Takahashi, K., Kiguchi, T., Sawasaki, Y., Karikusa, F., Nemoto, N., Matsuoka, T., and Yamamoto, M. (1992) Lung capillary endothelial cells produce and secrete urokinase-type plasminogen activator. *Am. J. Respir. Cell Mol. Biol.* **7,** 90–94
7. Chapman, H. A., Allen, C. L., and Stone, O. L. (1986) Abnormalities in pathways of alveolar fibrin turnover among patients with interstitial lung disease. *Am. Rev. Respir. Dis.* **133,** 437–443
8. Kotani, I., Sato, A., Hayakawa, H., Urano, T., Takada, Y., and Takada, A. (1995) Increased procoagulant and antifibrinolytic activities in the lungs with idiopathic pulmonary fibrosis. *Thromb. Res.* **77,** 493–504
9. Glas, G. J., Van Der Sluijs, K. F., Schultz, M. J., Hofstra, J. J., Van Der Poll, T., and Levi, M. (2013) Bronchoalveolar hemostasis in lung injury and acute respiratory distress syndrome. *J. Thromb. Haemost.* **11,** 17–25
10. Idell, S. (2008) The pathogenesis of pleural space loculation and fibrosis. *Curr. Opin. Pulm. Med.* **14,** 310–315
11. Idell, S., James, K. K., and Coalson, J. J. (1992) Fibrinolytic activity in bronchoalveolar lavage of baboons with diffuse alveolar damage: trends in two forms of lung injury. *Crit. Care Med.* **20,** 1431–1440
12. Idell, S., Zwieb, C., Kumar, A., Koenig, K. B., and Johnson, A. R. (1992) Pathways of fibrin turnover of human pleural mesothelial cells *in vitro*. *Am. J. Respir. Cell Mol. Biol.* **7,** 414–426
13. Viscardi, R. M., Broderick, K., Sun, C. C., Yale-Loehr, A. J., Hessamfar, A., Taciak, V., Burke, K. C., Koenig, K. B., and Idell, S. (1992) Disordered pathways of fibrin turnover in lung lavage of premature infants with respiratory distress syndrome. *Am. Rev. Respir. Dis.* **146,** 492–499
14. Idell, S., Koenig, K. B., Fair, D. S., Martin, T. R., McLarty, J., and Maunder, R. J. (1991) Serial abnormalities of fibrin turnover in evolving adult respiratory distress syndrome. *Am. J. Physiol.* **261,** L240–L248
15. Bertozzi, P., Astedt, B., Zenzius, L., Lynch, K., LeMaire, F., Zapol, W., and Chapman, H. A., Jr. (1990) Depressed bronchoalveolar urokinase activity in patients with adult respiratory distress syndrome. *N. Engl. J. Med.* **322,** 890–897
16. Prabhakaran, P., Ware, L. B., White, K. E., Cross, M. T., Matthay, M. A., and Olman, M. A. (2003) Elevated levels of plasminogen activator inhibitor-1 in pulmonary edema fluid are associated with mortality in acute lung injury. *Am. J. Physiol. Lung Cell Mol. Physiol.* **285,** L20–L28
17. Sisson, T. H., Hanson, K. E., Subbotina, N., Patwardhan, A., Hattori, N., and Simon, R. H. (2002) Inducible lung-specific urokinase expression reduces fibrosis and mortality after lung injury in mice. *Am. J. Physiol. Lung Cell Mol. Physiol.* **283,** L1023–L1032
18. Sapru, A., Curley, M. A., Brady, S., Matthay, M. A., and Flori, H. (2010) Elevated PAI-1 is associated with poor clinical outcomes in pediatric patients with acute lung injury. *Intensive Care Med.* **36,** 157–163
19. Matthay, M. A., Folkesson, H. G., and Clerici, C. (2002) Lung epithelial fluid transport and the resolution of pulmonary edema. *Physiol. Rev.* **82,** 569–600
20. Eaton, D. C., Helms, M. N., Koval, M., Bao, H. F., and Jain, L. (2009) The contribution of epithelial sodium channels to alveolar function in health and disease. *Annu. Rev. Physiol.* **71,** 403–423
21. Davis, I. C., and Matalon, S. (2007) Epithelial sodium channels in the adult lung-important modulators of pulmonary health and disease. *Adv. Exp. Med. Biol.* **618,** 127–140
22. Ji, H. L., Zhao, R. Z., Chen, Z. X., Shetty, S., Idell, S., and Matalon, S. (2012) δ ENaC: a novel divergent amiloride-inhibitable sodium channel. *Am. J. Physiol. Lung Cell Mol. Physiol.* **303,** L1013–L1026
23. Fuller, C. M., Ismailov, I. I., Berdiev, B. K., Shlyonsky, V. G., and Benos, D. J. (1996) Kinetic interconversion of rat and bovine homologs of the α subunit of an amiloride-sensitive Na^+ channel by C-terminal truncation of the bovine subunit. *J. Biol. Chem.* **271,** 26602–26608
24. Matthay, M. A. (2014) Resolution of pulmonary edema: thirty years of progress. *Am. J. Respir. Crit. Care Med.* **189,** 1301–1308
25. Hummler, E., and Planès, C. (2010) Importance of ENaC-mediated sodium transport in alveolar fluid clearance using genetically-engineered mice. *Cell Physiol. Biochem.* **25,** 63–70
26. Strange, C., Baumann, M. H., Sahn, S. A., and Idell, S. (1995) Effects of intrapleural heparin or urokinase on the extent of tetracycline-induced pleural disease. *Am. J. Respir. Crit. Care Med.* **151,** 508–515
27. Komissarov, A. A., Florova, G., Azghani, A., Karandashova, S., Kurdowska, A. K., and Idell, S. (2013) Active α-macroglobulin is a reservoir for urokinase after fibrinolytic therapy in rabbits with tetracycline-induced pleural injury and in human pleural fluids. *Am. J. Physiol. Lung Cell Mol. Physiol.* **305,** L682–L692
28. Renckens, R., Roelofs, J. J., Stegenga, M. E., Florquin, S., Levi, M., Carmeliet, P., Van't Veer, C., and van der Poll, T. (2008) Transgenic tissue-type plasminogen activator expression improves host defense during *Klebsiella pneumonia*. *J. Thromb. Haemost.* **6,** 660–668
29. Stringer, K. A., Hybertson, B. M., Cho, O. J., Cohen, Z., and Repine, J. E. (1998) Tissue plasminogen activator (tPA) inhibits interleukin-1 induced acute lung leak. *Free Radic. Biol. Med.* **25,** 184–188
30. Münster, A. M., Bendstrup, E., Jensen, J. I., and Gram, J. (2000) Jet and ultrasonic nebulization of single chain urokinase plasminogen activator (scu-PA). *J. Aerosol Med.* **13,** 325–333
31. Stringer, K. A., Dunn, J. S., and Gustafson, D. L. (2004) Administration of exogenous tissue plasminogen activator reduces oedema in mice lacking the tissue plasminogen activator gene. *Clin. Exp. Pharmacol. Physiol.* **31,** 327–330
32. Huang, L. T., Chou, H. C., Wang, L. F., and Chen, C. M. (2012) Tissue plasminogen activator attenuates ventilator-induced lung injury in rats. *Acta Pharmacol. Sin.* **33,** 991–997
33. Passero, C. J., Mueller, G. M., Rondon-Berrios, H., Tofovic, S. P., Hughey, R. P., and Kleyman, T. R. (2008) Plasmin activates epithelial Na^+ channels

by cleaving the γ subunit. *J. Biol. Chem.* **283,** 36586–36591
34. Haerteis, S., Krappitz, M., Diakov, A., Krappitz, A., Rauh, R., and Korbmacher, C. (2012) Plasmin and chymotrypsin have distinct preferences for channel activating cleavage sites in the γ subunit of the human epithelial sodium channel. *J. Gen. Physiol.* **140,** 375–389
35. Idell, S., Azghani, A., Chen, S., Koenig, K., Mazar, A., Kodandapani, L., Bdeir, K., Cines, D., Kulikovskaya, I., and Allen, T. (2007) Intrapleural low-molecular-weight urokinase or tissue plasminogen activator versus single-chain urokinase in tetracycline-induced pleural loculation in rabbits. *Exp. Lung Res.* **33,** 419–440
36. Idell, S., Allen, T., Chen, S., Koenig, K., Mazar, A., and Azghani, A. (2007) Intrapleural activation, processing, efficacy, and duration of protection of single-chain urokinase in evolving tetracycline-induced pleural injury in rabbits. *Am. J. Physiol. Lung Cell Mol. Physiol.* **292,** L25–L32
37. Kvassman, J. O., Lawrence, D. A., and Shore, J. D. (1995) The acid stabilization of plasminogen activator inhibitor-1 depends on protonation of a single group that affects loop insertion into β-sheet A. *J. Biol. Chem.* **270,** 27942–27947
38. Ji, H. L., and Benos, D. J. (2004) Degenerin sites mediate proton activation of δβγ-epithelial sodium channel. *J. Biol. Chem.* **279,** 26939–26947
39. Molina, R., Han, D. Y., Su, X. F., Zhao, R. Z., Zhao, M., Sharp, G. M., Chang, Y., and Ji, H. L. (2011) Cpt-cAMP activates human epithelial sodium channels via relieving self-inhibition. *Biochim. Biophys. Acta* **1808,** 1818–1826
40. Ji, H. L., Parker, S., Langloh, A. L., Fuller, C. M., and Benos, D. J. (2001) Point mutations in the post-M2 region of human α-ENaC regulate cation selectivity. *Am. J. Physiol. Cell Physiol.* **281,** C64–C74
41. Ji, H. L., Su, X. F., Kedar, S., Li, J., Barbry, P., Smith, P. R., Matalon, S., and Benos, D. J. (2006) δ-Subunit confers novel biophysical features to αβγ-human epithelial sodium channel (ENaC) via a physical interaction. *J. Biol. Chem.* **281,** 8233–8241
42. Haerteis, S., Krueger, B., Korbmacher, C., and Rauh, R. (2009) The δ-subunit of the epithelial sodium channel (ENaC) enhances channel activity and alters proteolytic ENaC activation. *J. Biol. Chem.* **284,** 29024–29040
43. Ke, S. H., Coombs, G. S., Tachias, K., Corey, D. R., and Madison, E. L. (1997) Optimal subsite occupancy and design of a selective inhibitor of urokinase. *J. Biol. Chem.* **272,** 20456–20462
44. Ke, S. H., Coombs, G. S., Tachias, K., Navre, M., Corey, D. R., and Madison, E. L. (1997) Distinguishing the specificities of closely related proteases: role of P3 in substrate and inhibitor discrimination between tissue-type plasminogen activator and urokinase. *J. Biol. Chem.* **272,** 16603–16609
45. Coombs, G. S., Bergstrom, R. C., Madison, E. L., and Corey, D. R. (1998) Directing sequence-specific proteolysis to new targets: the influence of loop size and target sequence on selective proteolysis by tissue-type plasminogen activator and urokinase-type plasminogen activator. *J. Biol. Chem.* **273,** 4323–4328
46. Ding, L., Coombs, G. S., Strandberg, L., Navre, M., Corey, D. R., and Madison, E. L. (1995) Origins of the specificity of tissue-type plasminogen activator. *Proc. Natl. Acad. Sci. U.S.A.* **92,** 7627–7631
47. Madison, E. L., Coombs, G. S., and Corey, D. R. (1995) Substrate specificity of tissue type plasminogen activator: characterization of the fibrin independent specificity of t-PA for plasminogen. *J. Biol. Chem.* **270,** 7558–7562
48. Verspurten, J., Gevaert, K., Declercq, W., and Vandenabeele, P. (2009) SitePredicting the cleavage of proteinase substrates. *Trends Biochem. Sci.* **34,** 319–323
49. Sherwood, T. W., Frey, E. N., and Askwith, C. C. (2012) Structure and activity of the acid-sensing ion channels. *Am. J. Physiol. Cell Physiol.* **303,** C699–C710
50. Jasti, J., Furukawa, H., Gonzales, E. B., and Gouaux, E. (2007) Structure of acid-sensing ion channel 1 at 1.9 Å resolution and low pH. *Nature* **449,** 316–323
51. Gonzales, E. B., Kawate, T., and Gouaux, E. (2009) Pore architecture and ion sites in acid-sensing ion channels and P2X receptors. *Nature* **460,** 599–604
52. Zeslawska, E., Jacob, U., Schweinitz, A., Coombs, G., Bode, W., and Madison, E. (2003) Crystals of urokinase type plasminogen activator complexes reveal the binding mode of peptidomimetic inhibitors. *J. Mol. Biol.* **328,** 109–118
53. Ji, H. L., Fuller, C. M., and Benos, D. J. (1999) Peptide inhibition of constitutively activated epithelial Na^+ channels expressed in *Xenopus* oocytes. *J. Biol. Chem.* **274,** 37693–37704
54. Sedý, J., Zicha, J., Kunes, J., Jendelová, P., and Syková, E. (2008) Mechanisms of neurogenic pulmonary edema development. *Physiol. Res.* **57,** 499–506
55. Ware, L. B., and Matthay, M. A. (2005) Clinical practice: acute pulmonary edema. *N. Engl. J. Med.* **353,** 2788–2796
56. Bhattacharya, J., and Matthay, M. A. (2013) Regulation and repair of the alveolar-capillary barrier in acute lung injury. *Annu. Rev. Physiol.* **75,** 593–615
57. MacLaren, R., and Jung, R. (2002) Stress-dose corticosteroid therapy for sepsis and acute lung injury or acute respiratory distress syndrome in critically ill adults. *Pharmacotherapy* **22,** 1140–1156
58. Pechlaner, C. (2002) Plasminogen activators in inflammation and sepsis. *Acta Med. Austriaca* **29,** 80–88
59. Stewart, R. J., Fredenburgh, J. C., Leslie, B. A., Keyt, B. A., Rischke, J. A., and Weitz, J. I. (2000) Identification of the mechanism responsible for the increased fibrin specificity of TNK-tissue plasminogen activator relative to tissue plasminogen activator. *J. Biol. Chem.* **275,** 10112–10120
60. Chraïbi, A., and Horisberger, J. D. (2002) Na self inhibition of human epithelial Na channel: temperature dependence and effect of extracellular proteases. *J. Gen. Physiol.* **120,** 133–145
61. Sheng, S., Maarouf, A. B., Bruns, J. B., Hughey, R. P., and Kleyman, T. R. (2007) Functional role of extracellular loop cysteine residues of the epithelial Na^+ channel in Na^+ self-inhibition. *J. Biol. Chem.* **282,** 20180–20190
62. Sheng, S., Perry, C. J., and Kleyman, T. R. (2004) Extracellular Zn^{2+} activates epithelial Na^+ channels by eliminating Na^+ self-inhibition. *J. Biol. Chem.* **279,** 31687–31696
63. Caldwell, R. A., Boucher, R. C., and Stutts, M. J. (2005) Neutrophil elastase activates near-silent epithelial Na^+ channels and increases airway epithelial Na^+ transport. *Am. J. Physiol. Lung Cell Mol. Physiol.* **288,** L813–L819
64. Caldwell, R. A., Boucher, R. C., and Stutts, M. J. (2004) Serine protease activation of near-silent epithelial Na^+ channels. *Am. J. Physiol. Cell Physiol.* **286,** C190–C194
65. Diakov, A., Bera, K., Mokrushina, M., Krueger, B., and Korbmacher, C. (2008) Cleavage in the γ-subunit of the epithelial sodium channel (ENaC) plays an important role in the proteolytic activation of near-silent channels. *J. Physiol.* **586,** 4587–4608
66. Goldfarb, S. B., Kashlan, O. B., Watkins, J. N., Suaud, L., Yan, W., Kleyman, T. R., and Rubenstein, R. C. (2006) Differential effects of Hsc70 and Hsp70 on the intracellular trafficking and functional expression of epithelial sodium channels. *Proc. Natl. Acad. Sci. U.S.A.* **103,** 5817–5822
67. Rossier, B. C. (2004) The epithelial sodium channel: activation by membrane-bound serine proteases. *Proc. Am. Thorac. Soc.* **1,** 4–9
68. Rossier, B. C., and Stutts, M. J. (2009) Activation of the epithelial sodium channel (ENaC) by serine proteases. *Annu. Rev. Physiol.* **71,** 361–379
69. Kleyman, T. R., Carattino, M. D., and Hughey, R. P. (2009) ENaC at the cutting edge: regulation of epithelial sodium channels by proteases. *J. Biol. Chem.* **284,** 20447–20451
70. Planès, C., and Caughey, G. H. (2007) Regulation of the epithelial Na^+ channel by peptidases. *Curr. Top. Dev. Biol.* **78,** 23–46
71. Neitzel, J. J. (2010) Enzyme catalysis: the serine proteases. *Nat. Educ.* **3,** 21
72. Knight, K. K., Wentzlaff, D. M., and Snyder, P. M. (2008) Intracellular sodium regulates proteolytic activation of the epithelial sodium channel. *J. Biol. Chem.* **283,** 27477–27482
73. García-Caballero, A., Dang, Y., He, H., and Stutts, M. J. (2008) ENaC proteolytic regulation by channel-activating protease 2. *J. Gen. Physiol.* **132,** 521–535
74. Idell, S., Girard, W., Koenig, K. B., McLarty, J., and Fair, D. S. (1991) Abnormalities of pathways of fibrin turnover in the human pleural space. *Am. Rev. Respir. Dis.* **144,** 187–194
75. Idell, S., James, K. K., Levin, E. G., Schwartz, B. S., Manchanda, N., Maunder, R. J., Martin, T. R., McLarty, J., and Fair, D. S. (1989) Local abnormalities in coagulation and fibrinolytic pathways predispose to alveolar fibrin deposition in the adult respiratory distress syndrome. *J. Clin. Invest.* **84,** 695–705

76. Kunzelmann, K., Beesley, A. H., King, N. J., Karupiah, G., Young, J. A., and Cook, D. I. (2000) Influenza virus inhibits amiloride-sensitive Na^+ channels in respiratory epithelia. *Proc. Natl. Acad. Sci. U.S.A.* **97,** 10282–10287
77. Chen, X. J., Seth, S., Yue, G., Kamat, P., Compans, R. W., Guidot, D., Brown, L. A., Eaton, D. C., and Jain, L. (2004) Influenza virus inhibits ENaC and lung fluid clearance. *Am. J. Physiol. Lung Cell Mol. Physiol.* **287,** L366–L373
78. Dagenais, A., Gosselin, D., Guilbault, C., Radzioch, D., and Berthiaume, Y. (2005) Modulation of epithelial sodium channel (ENaC) expression in mouse lung infected with *Pseudomonas aeruginosa*. *Respir. Res.* **6,** 2
79. Hochberg, I., Abassi, Z., and Azzam, Z. S. (2008) Patterns of alveolar fluid clearance in heart failure. *Int. J. Cardiol.* **130,** 125–130
80. Maron, M. B., Luther, D. J., Pilati, C. F., Ohanyan, V., Li, T., Koshy, S., Horne, W. I., Meszaros, J. G., Walro, J. M., and Folkesson, H. G. (2009) β-Adrenoceptor stimulation of alveolar fluid clearance is increased in rats with heart failure. *Am. J. Physiol. Lung Cell Mol. Physiol.* **297,** L487–L495
81. Chen, Z., Zhao, R., Zhao, M., Liang, X., Bhattarai, D., Dhiman, R., Shetty, S., Idell, S., and Ji, H. L. (2014) Regulation of epithelial sodium channels in urokinase plasminogen activator deficiency. *Am. J. Physiol. Lung Cell Mol. Physiol.* **307,** L609–L617
82. Crippa, M. P. (2007) Urokinase-type plasminogen activator. *Int. J. Biochem. Cell Biol.* **39,** 690–694
83. Ware, L. B., Camerer, E., Welty-Wolf, K., Schultz, M. J., and Matthay, M. A. (2006) Bench to bedside: targeting coagulation and fibrinolysis in acute lung injury. *Am. J. Physiol. Lung Cell Mol. Physiol.* **291,** L307–L311
84. Schuliga, M., Westall, G., Xia, Y., and Stewart, A. G. (2013) The plasminogen activation system: new targets in lung inflammation and remodeling. *Curr. Opin. Pharmacol.* **13,** 386–393
85. Bouros, D., Schiza, S., Tzanakis, N., Drositis, J., and Siafakas, N. (1996) Intrapleural urokinase in the treatment of complicated parapneumonic pleural effusions and empyema. *Eur. Respir. J.* **9,** 1656–1659
86. Lee, K. S., Im, J. G., Kim, Y. H., Hwang, S. H., Bae, W. K., and Lee, B. H. (1991) Treatment of thoracic multiloculated empyemas with intracavitary urokinase: a prospective study. *Radiology* **179,** 771–775
87. Günther, A., Lübke, N., Ermert, M., Schermuly, R. T., Weissmann, N., Breithecker, A., Markart, P., Ruppert, C., Quanz, K., Ermert, L., Grimminger, F., and Seeger, W. (2003) Prevention of bleomycin-induced lung fibrosis by aerosolization of heparin or urokinase in rabbits. *Am. J. Respir. Crit. Care Med.* **168,** 1358–1365
88. Kuramoto, E., Nishiuma, T., Kobayashi, K., Yamamoto, M., Kono, Y., Funada, Y., Kotani, Y., Sisson, T. H., Simon, R. H., and Nishimura, Y. (2009) Inhalation of urokinase-type plasminogen activator reduces airway remodeling in a murine asthma model. *Am. J. Physiol. Lung Cell Mol. Physiol.* **296,** L337–L346
89. Schermuly, R. T., Günther, A., Ermert, M., Ermert, L., Ghofrani, H. A., Weissmann, N., Grimminger, F., Seeger, W., and Walmrath, D. (2001) Conebulization of surfactant and urokinase restores gas exchange in perfused lungs with alveolar fibrin formation. *Am. J. Physiol. Lung Cell Mol. Physiol.* **280,** L792–L800
90. Komissarov, A. A., Florova, G., Azghani, A., Karandashova, S., Kurdowska, A. K., and Idell, S. (2013) Active α-macroglobulin is a reservoir for urokinase after fibrinolytic therapy in rabbits with tetracycline-induced pleural injury and in human pleural fluids. *Am. J. Physiol. Lung Cell Mol. Physiol.* **305,** L682–L692
91. Komissarov, A. A., Mazar, A. P., Koenig, K., Kurdowska, A. K., and Idell, S. (2009) Regulation of intrapleural fibrinolysis by urokinase-α-macroglobulin complexes in tetracycline-induced pleural injury in rabbits. *Am. J. Physiol. Lung Cell Mol. Physiol.* **297,** L568–L577
92. Miyake, H., Hara, I., Yamanaka, K., Gohji, K., Arakawa, S., and Kamidono, S. (1999) Elevation of serum levels of urokinase-type plasminogen activator and its receptor is associated with disease progression and prognosis in patients with prostate cancer. *Prostate* **39,** 123–129